applied sciences

MDPI

Article

Experimental Study on Bearing Capacity of Compression Members of Space Grid Structures Reinforced by RPC

Yutong Duan, Honggang Lei *, Yan Zhou and Shihong Jin

College of Civil Engineering, Taiyuan University of Technology, Taiyuan 030024, China; dytong163@163.com (Y.D.); 18234132947@163.com (Y.Z.); jsh-dt-ty@163.com (S.J.)
* Correspondence: lhgang168@126.com

Abstract: Insufficient bearing capacity of compression bars in space grid structures can significantly reduce the collapse resistance of structures and cause immeasurable losses. Reactive powder concrete (RPC) with high strength, micro-expansion, and good ductility is used to reinforce the compression members of grid structures by infilling steel tubes. Axial compression tests on five types of high-frequency welded pipes with different section sizes and initial stresses were carried out. The results showed that compared to steel tubes alone, the bearing capacity of steel tubes reinforced by RPC could be increased by 75.77 to 218.34%. With a decrease of either the initial stress or confinement coefficient, the contribution of the material reinforcement increased. The failure mode of the specimen after RPC grouting was the same as that of the non-reinforced steel pipe, which was dominated by elastic-plastic buckling. The grouting hole after reinforcement did not fail prior to the instability of the member, which suggests that necessary measures to repair the hole should be taken. Based on the design method of axial compression bearing capacity of concrete-filled steel tubular members in six codes in China and abroad, the test results of this paper and 242 RPC-filled steel tubes were compared and analyzed. Finally, an equation of nominal bearing capacity, which estimates the ultimate bearing capacity of compressive members strengthened by filled RPC in grid structures, was proposed.

Keywords: space grid structure; RPC filling reinforcement; axial compression; initial stress; ultimate bearing capacity

Citation: Duan, Y.; Lei, H.; Zhou, Y.; Jin, S. Experimental Study on Bearing Capacity of Compression Members of Space Grid Structures Reinforced by RPC. *Appl. Sci.* **2022**, *12*, 7809. https://doi.org/10.3390/app12157809

Academic Editor: Pier Paolo Rossi

Received: 17 June 2022
Accepted: 2 August 2022
Published: 3 August 2022

1. Introduction

The spatial grid structure's (Figure 1) characteristics of large space, lightweight, and firmness enable designers to apply it in continuous innovation and exploration [1,2]. It can be traced back to the early 20th century when a prototype of a small space grid structure formed by the combination of several triangular and quadrangular pyramid elements was developed by the American inventor Alexander Graham Bell. As a highly modular statically indeterminate structure, the spatial grid is beautiful in shape, reasonable in strength, and variable in form, which fully meets the professional requirements of architects and structural engineers. Therefore, the spatial grid is widely used in public and industrial buildings, such as convention and exhibition centers, gymnasiums, waiting halls, hangars, and dry coal sheds [3].

As shown in Figure 2, due to the abnormal design [4], construction [4–6], use [7,8], and the need for subsequent functional upgrading and transformation, the spatial grid structure contains a large number of congenital defects, which can result in long-term cumulative damage and overload. If the bearing capacity does not meet the safety and use requirements of the current regulations, accidents involving the collapse of the structure are not uncommon [9–11]. Therefore, reinforcing the bearing capacity of an in-service spatial grid structure has become an important discussion topic in academic and engineering circles.

(**a**)

(**b**)

(**c**)

Figure 1. Space frame structures. (**a**) Space truss; (**b**) Latticed shell; (**c**) Spatial truss.

As an axial force system, the members of a space grid structure are divided into axial compression and axial tension, characterized by a large aspect ratio, small steel pipe section size, and high-frequency-welded pipe applications. The method put forward in this paper of strengthening the compression bars of a grid structure is based on steel tube strengthening with filled concrete from "Steel Structure Reinforcement Design Standard" GB 51367-2019 [12]. This standard technique requires pouring a lightweight and high-strength cement-based material into the steel pipe through a grouting hole bored in the tube. The research on the mechanical properties of concrete-filled steel tubes [13,14] has matured, and the selection of infill concrete has gradually shifted from ordinary concrete to ultra-high strength concrete [14,15]. Considering the size of the grouting hole, reactive powder concrete (RPC) [16] with ultra-high strength, micro-expansion, no coarse aggregate, and excellent durability was selected as the filling material in this paper.

Research on RPC-filled steel pipes primarily includes axial compression [17,18], axial tension [19], bending resistance [20], compression bending [20,21], and stability [22]; and several design methods have been proposed. Existing research on concrete-filled steel tubular (CFST) grid structures [23–26] show that as the self-weight of the CFST grid increases, the stiffness and ultimate bearing capacity of the grid frame improves significantly, and it exhibits good seismic performance compared to a non-reinforced grid structure of the same design. Using CFST for grid design reduces the amount of steel required. The overall cost can be reduced by more than 30%, which demonstrates its excellent economic benefits

and mechanical properties and provides strong evidence for the application of the internal pouring of concrete reinforcement method in the grid structure.

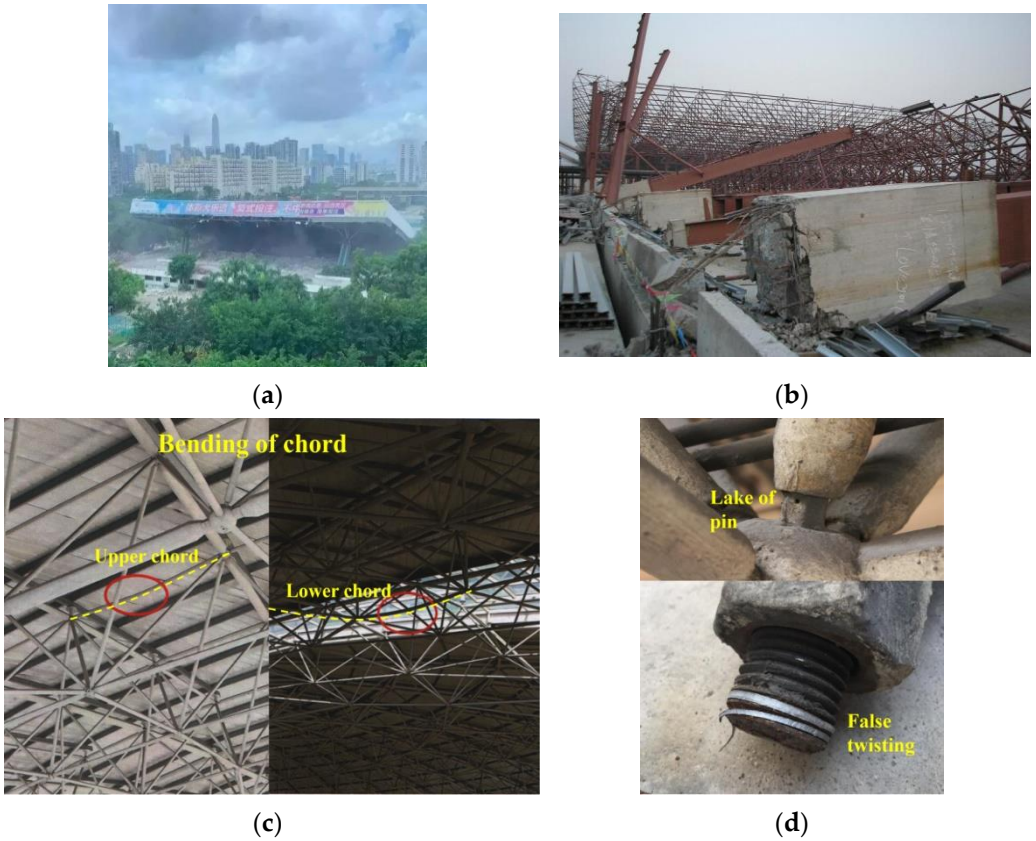

Figure 2. Accidents and abnormal cases in the space frame structure. (**a**) Gymnasium collapse; (**b**) Convention center collapse; (**c**) Member defect; (**d**) Joint defect [6].

Seamless steel pipes are mostly used in axial compression performance tests of RPC-filled steel tubes. Additionally, the specimen size is not commonly used in the grid structure, being significantly shorter than the length in the grid structure. Duan and Lei [27] showed that the 10 Chinese codes involving CFST stipulate that the minimum diameter of the circular pipe should be no less than 168 mm, and the length-to-diameter ratio should not be greater than 20. The structural requirements and design methods of CFST members, given by neither the "Technical code for concrete filled steel tubular structures" GB 50936-2014 [28] nor the "Standard for the design of strengthening steel structure" GB 51367-2019 [12], can be directly applied to grid structure members. The difference in mechanical properties between RPC and ordinary concrete makes it no longer suitable for the existing design and calculation methods of CFST members [29,30]. Thus, 25 tests on the axial compression performance of members with the common cross-section of a grid structure were designed to verify the feasibility of the reinforcement method proposed in this paper. The objectives of this work also include: studying the load-deformation curve, stress-strain change law, and failure mode, analyzing the influence of the initial stress of the in-service members on the reinforcement effect, listing the structural requirements and design methods of the axial compression bearing capacity of composite members in six domestic and foreign codes, and comparing the test results of this paper with 242 outcomes from different scholars and the estimated bearing capacity from illustrated codes. The equations for predicting the load capacity of the compression members in grid structure reinforcing by filling with RPC will then be proposed.

2. Experimental Program

2.1. Specimen Design

A total of 25 axial compression tests were conducted. The test parameters include the diameter, confinement coefficient, section form, and initial stress of the steel pipe. The section sizes of the steel pipes in this paper were selected as ⌀60 × 3.5, ⌀75.5 × 3.75, ⌀88.5 × 4, ⌀114 × 4, and ⌀159 × 6 mm. Each group included five types of specimens: steel pipe (S-IS0), concrete-filled steel tube (RS-IS0), and concrete-filled steel tubes with initial stress ratios of 0.4 (RS-IS4), 0.6 (RS-IS6), and 0.8 (RS-IS8). GB 50936-2014 [28] stipulates that the axial stress of a steel pipe should not be greater than 60% of the design value of the compressive strength of the pipe before filling with concrete and that the pipe must still meet stability requirements. Therefore, the initial stress ratios of the tested components were 0.4, 0.6, and 0.8. The steel pipe used was Q235B, a high-frequency welded pipe, and the inner filling concrete was RPC100 produced by Tianjin Keen Construction Technology Co., Ltd. in Tianjin, China. As the length-to-diameter ratio (L/D) of CFST increased between 4 and 5, the specimen gradually changed from strength failure to elastic-plastic instability failure, and when L/D $\geq$ 6, it showed apparent instability failure [31]. Regarding the test conditions and specimen size, the length of each specimen was set to 1.5 m, and the length-to-diameter ratio was between 6.60 and 17.5. The specimen parameters are shown in Table 1.

Table 1. Summary of main specimen parameters.

Specimen	$D \times t \times L$ (mm)	L_e/D	f_y (MPa)	f_c (MPa)	ξ
S-IS0-60	60 × 3.5 × 1500	17.5	403	-	-
RS-IS0-60					
RS-IS4-60			403	100	1.13
RS-IS6-60					
RS-IS8-60					
S-IS0-75.5	75.5 × 3.75 × 1500	13.91	387	-	-
RS-IS0-75.5					
RS-IS4-75.5			387	100	0.90
RS-IS6-75.5					
RS-IS8-75.5					
S-IS0-88.5	88.5 × 4 × 1500	11.86	368	-	-
RS-IS0-88.5					
RS-IS4-88.5			368	100	0.76
RS-IS6-88.5					
RS-IS8-88.5					
S-IS0-114	114 × 4 × 1500	9.21	326	-	-
RS-IS0-114					
RS-IS4-114			326	100	0.51
RS-IS6-114					
RS-IS8-114					
S-IS0-159	159 × 6 × 1500	6.60	410	-	-
RS-IS0-159					
RS-IS4-159			410	100	0.69
RS-IS6-159					
RS-IS8-159					

Note: D and t represent the diameter and thickness of the pipe. L_e is the effective length of the pipe, which values 0.7 L according to the test boundary conditions. f_y and f_c denote the yield strength of the steel pipe and the compressive design strength of RPC, respectively. ξ is the confinement coefficient, $\xi = A_s f / A_c f_c$.

2.2. Specimen Making

2.2.1. Preliminary Processing

The specimens were subjected to full-section compression loading. The basic components of all specimens comprised a 1500 mm long circular steel tube with a rectangular terminal plate welded to each end. For the CFST specimen without initial stress, a filling hole with a diameter of 50 mm was set in the center of one end plate. The initial stress test

pieces needed bolt holes with diameters of 32 mm in the four corners of the terminal plate and penetrated by four steel rods, as shown in Figure 3.

Figure 3. Specimens fabricated in the factory.

2.2.2. Prestress Applying

A torque wrench was used to tighten the nuts at both ends of the specimen to apply an initial pressure to the steel pipe (Figure 4), calculated in accordance with Clause 7.2.1 of GB 50017-2017 [32]. The initial pressure put on the tube was the product of the bearing capacity of the steel tube and the initial stress ratio. During the tightening, the strain values on the rod and steel tube were monitored to ensure that the initial pressure was applied to the expected value. The load was supplemented over time after the first loading until the RPC in the tube was initially solidified.

Figure 4. Preload applying.

2.2.3. RPC Grouting

First, the center of the grouting hole was marked 100 mm from the terminal plate on one side, and an electric drill was used to perforate a grouting hole with the target size on the steel pipe. To reduce the damage caused by the tapping of the pipe, only one grouting hole was drilled into the pipe, which also served as an exhaust hole. Secondly, the specimen was placed horizontally to simulate the upper and lower chords of the space structure in service. To help the gas in the tube exhaust promptly, a funnel was placed 5–10 mm above the hole while grouting. Then the mixed RPC was poured slowly into the pipe through the funnel at a constant speed. Due to the excellent fluidity of RPC, no blockage or stagnation

was found during the filling process. Finally, if there was no crisp, hollow sound when knocking on the pipe surface, the material in the tube was assumed to be relatively dense.

RPC exhibits excellent properties under steam curing conditions; however, its compressive strength under natural curing can only reach up to 75–85% of the steam curing maximum [33]. Considering that it is difficult to achieve high-temperature curing during the reinforcement process, the specimens were naturally cured for 28 d at normal temperature after sealing the hole with cling film.

To avoid local buckling at the grouting hole, a quadrilateral arc plate cut from the same diameter steel tube was used to repair the hole by bonding it to the steel tube using steel glue with a thickness of approximately 2 mm. The grouting process as shown in Figure 5.

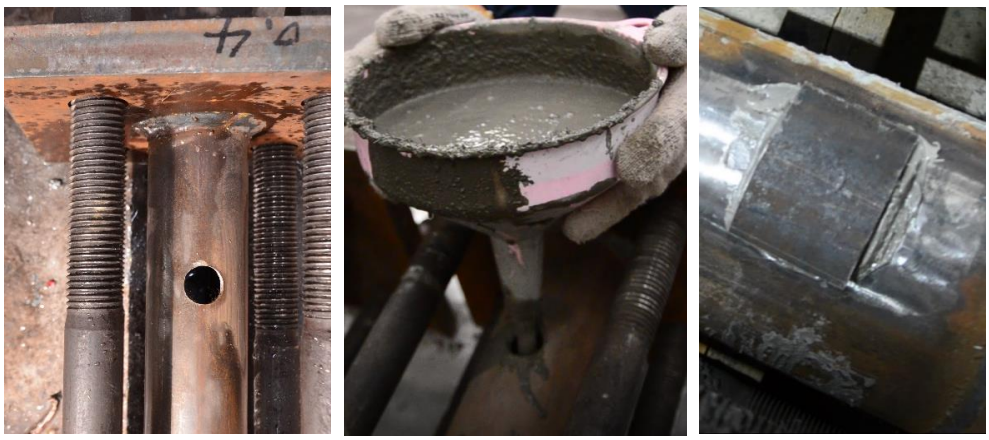

(**a**) (**b**) (**c**)

Figure 5. RPC grouting. (**a**) Trepanning; (**b**) Grouting; (**c**) Strengthening.

2.3. Material Properties

2.3.1. Steel

Three arc-shaped standard longitudinal tensile specimens were made for each of five steel pipe sizes (Figure 6). Their mechanical properties, including yield strength and ultimate strength, were tested according to "Metallic materials- Tensile testing-Part 1: Method of test at room temperature" GB/T 228.1-2010 [34] and "Steel and steel products-Location and the preparation of samples and test pieces for mechanical testing" GB/T 2975-2018 [35]. The test results are shown in Table 2.

(**a**) (**b**) (**c**)

Figure 6. Steel pipe material sample. (**a**) Sampling location; (**b**) Tensile specimen; (**c**) Material test.

2.3.2. RPC

Test cubes with dimensions 100 mm × 100 mm × 100 mm, 100 mm × 100 mm × 300 mm, and 60 mm × 13 mm × 320 mm (Figure 7).were prepared to determine the strength of RPC in accordance with "Reactive powder concrete" GB/T 31387-2015 [36] and "Standard for

test methods of concrete physical and mechanical properties" GB/T 50081-2019 [37]. The testing included cube compressive strength, f_{cu}, at 3, 7, and 28 days; axial compressive strength, f_c; elastic modulus, E_c; and axial tensile strength, f_t. Each group had three test blocks except the tensile strength test, which contained six blocks. The test blocks were wrapped with preservative film after demolding to simulate the curing condition of RPC poured into a steel tube which would be closed natural curing at normal temperature. The test results are shown in Table 3.

Table 2. Mechanical performance test results of steel pipes.

Number	Specimen	Yield Strength f_y (N/mm^2)	Ultimate Strength f_u (N/mm^2)	Percentage Elongation after Fracture δ	Yield Ratio
1	T60	403.92	545.38	22.13	0.74
2	T75.5	387.80	518.23	22.50	0.74
3	T88.5	368.94	509.36	21.98	0.72
4	T114	326.46	474.40	24.92	0.70
5	T159	410.95	592.14	26.58	0.70

(**a**) (**b**) (**c**)

Figure 7. RPC material sample. (**a**) Compressive; (**b**) Uniaxial compressive; (**c**) Tension.

Table 3. Mechanical performance test results of RPC.

Cube Strength f_{cu} (N/mm^2)			Axial Compressive Strength f_c (N/mm^2)	Tensile Strength f_t (N/mm^2)	Young's Modulus E_c (N/mm^2)
3 d	7 d	28 d			
95.29	107.26	125.56	100.49	6.46	3.95×10^4

2.4. Test Setup and Instrumentation

As shown in Figures 8 and 9, the instruments used in the test included a 5000 kN microcomputer controlled electro-hydraulic servo pressure testing machine, 4 linear variable displacement transducers (LVDT), and 16 strain gauges (at 8 survey points). The main measurements of this test were the overall vertical deformation of the specimen, the horizontal displacement of the specimen, and the longitudinal and hoop strains of the pipe surface. Two LVDTs were arranged symmetrically between the upper and lower loading plates to measure the overall vertical deformation, and two horizontal LVDTs were arranged at 200 and 750 mm from one end along the length of the steel pipe to measure the lateral deflection of the specimen. Applying the previous test results, the arrangement of the horizontal displacement gauge was adjusted to measure two directions in the middle of the steel pipe. Four pairs of mutually perpendicular strain gauges were evenly arranged around both the midspan and grouting hole of the initial stress specimens to measure the longitudinal and hoop strains on the pipe surface.

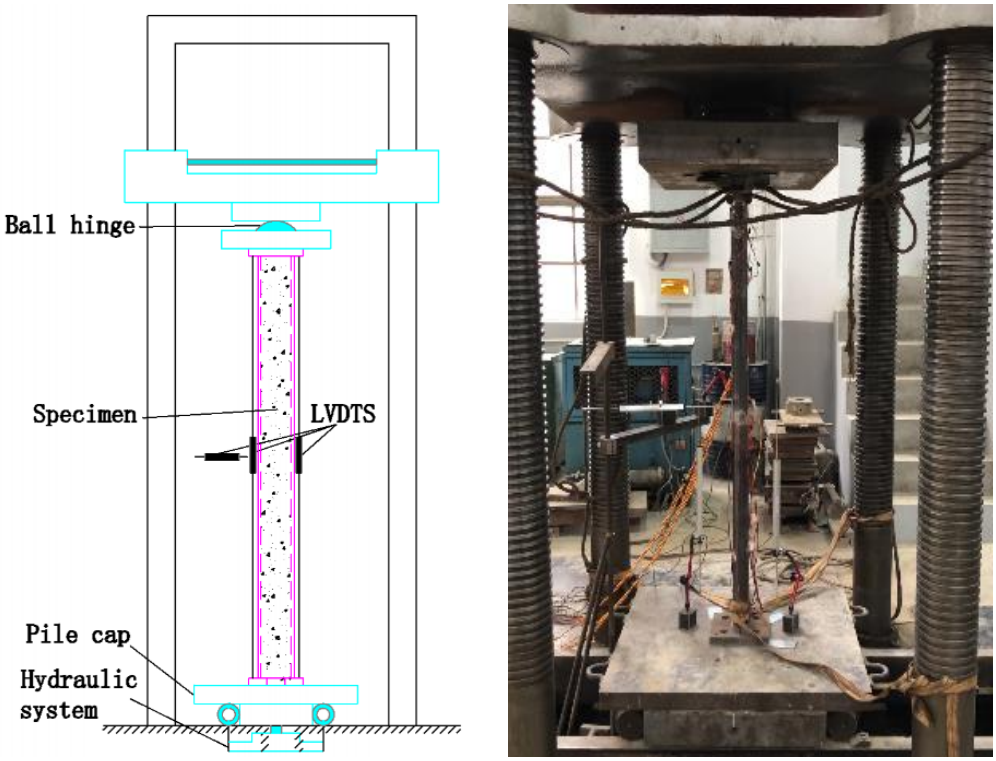

Figure 8. Test setup.

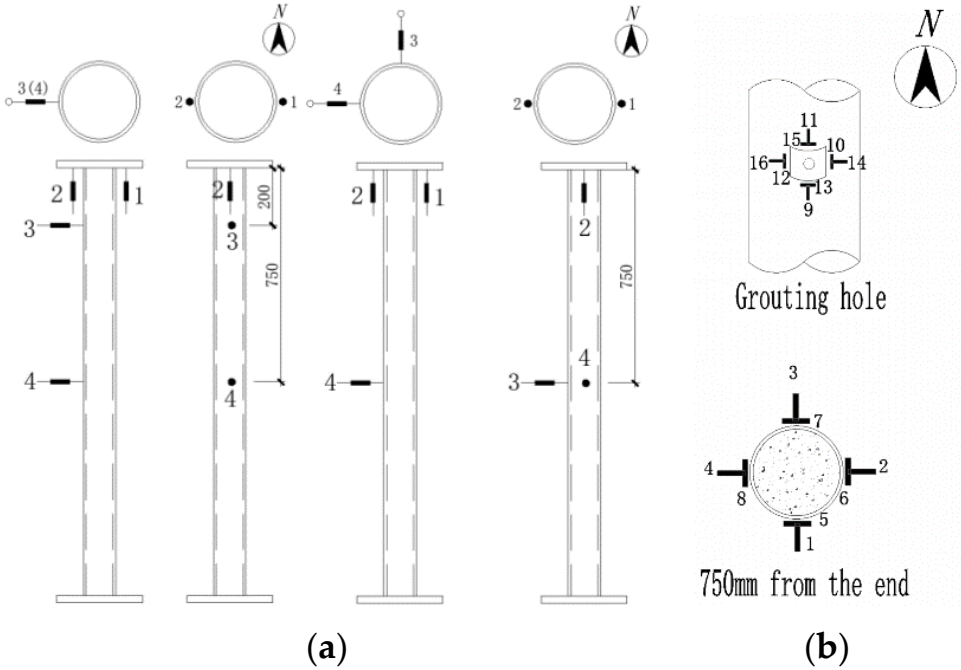

Figure 9. Arrangements of instrumentation. (**a**) LVDTs; (**b**) Strain gauges.

2.5. Loading System

A load control divided into seven stages was adopted until the test load reached 70% of the predicted bearing capacity. Then a displacement control mode with the velocity of loading applied at 0.002–0.005 mm/s was adopted until the load decreased to 75% of the ultimate bearing capacity or the deformation was too large.

3. Experimental Results

This section may be divided into subheadings. It should provide a concise and precise description of the experimental results, their interpretation, and the experimental conclusions that can be drawn.

3.1. Failure Mode

For the steel pipe specimens in Figure 10, little horizontal displacement and no obvious deformation were observed at the preliminary loading stage. Upon reaching the peak load, the horizontal displacement in the middle of the specimen increased nonlinearly, and the bearing capacity of the specimen decreased gradually with lateral bending occurring in the horizontal displacement plane until it lost its overall stability.

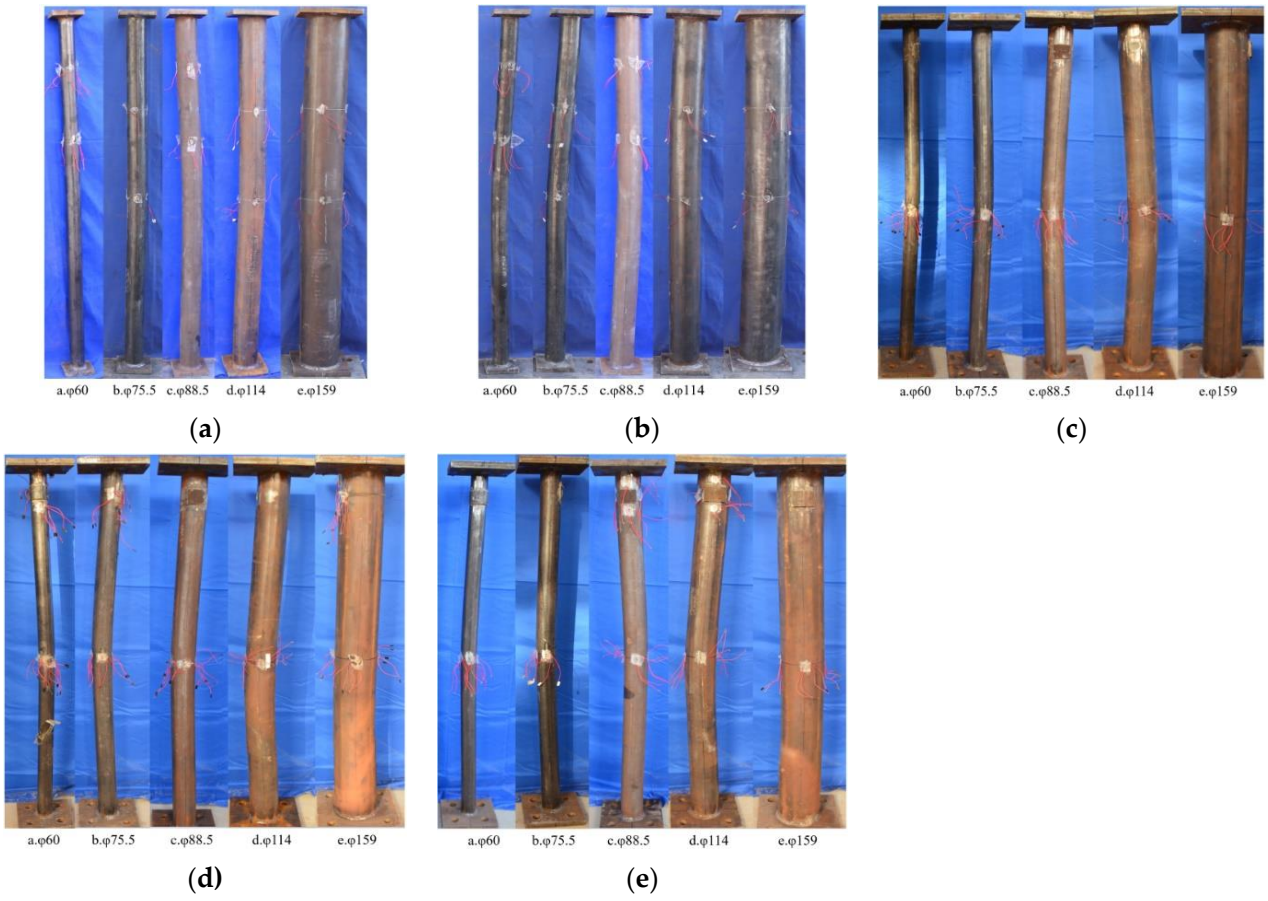

Figure 10. The overall failure mode of the specimen by type. (**a**) Non-reinforced, IS0; (**b**) IS0; (**c**) IS4; (**d**) IS6; (**e**) IS8.

All the CFST specimens without prestress presented elastoplastic instability failure, with more significant lateral bending occurring in the middle of the specimens at small diameters. Low horizontal displacement was produced at the elastic stage and increased slowly with the load raising before it developed rapidly after reaching the peak load. Similarly, instability in the steel pipes appeared when the specimen failed.

The CFST specimens with prestress exhibited little difference from non-prestress members, with the failure mode still dominated by instability at the peak load. The initial stress caused the reinforced steel pipes to enter the plastic stage in advance, which occurred earlier under larger initial stress. For specimens with larger diameters and relatively smaller aspect ratios, the early plastic state of the steel pipe reduced its connection to the RPC, and local buckling accompanied by oblique shear failure occurred at the bottom of the specimen in the bearing capacity decline section, as shown in Figure 11. The strengthening

measure around the grouting hole ensured that local buckling occurred there later than the overall instability, though tiny cracks in the steel adhesive around the reinforced arc plate appeared for most specimens, and a few reinforced arc plates peeled off, which resulted in a small area of crippling at the edge of the grouting hole.

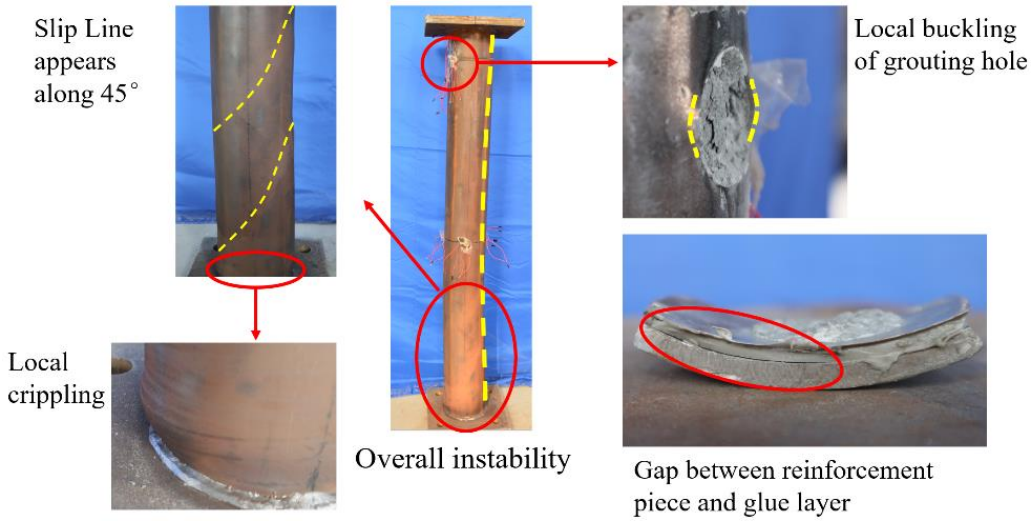

Figure 11. Typical failure mode in descending branch of load-displacement curves.

3.2. Load Capacities

The test results in Table 4 show the test bearing capacity N_e, value of bearing capacity N_c estimated by GB 50017-2017 [32] for steel pipes, GB 51367-2019 [12], and GB 50936-2014 [28] for specimens with and without initial stress, respectively, and the percentage of the added bearing capacity of the members strengthened by RPC compared with the pure steel tube, which is defined as the reinforcement material contribution RP (Reinforced Percentage) as follows:

$$RP = \frac{N_{sc} - N_s}{N_s} \times 100\% \quad (1)$$

where N_{sc} and N_s are the test bearing capacity of concrete-filled steel tubes and steel pipes, respectively.

Table 4. Test results of ultimate bearing capacity (kN).

Specimen	N_e	N_c	Error (%)	*RP* (%)	Specimen	N_e	N_c	Error (%)	*RP* (%)
S-IS0-60	196.59	211	−6.8		S-IS0-75.5	270.39	292	−7.4	
RS-IS0-60	345.54	444	28.4	75.77	RS-IS0-75.5	604.22	735	21.7%	123.46
RS-IS4-60	276.31	355	28.5	40.55	RS-IS4-75.5	494.64	588	18.9%	82.94
RS-IS6-60	249.77	333	33.2	27.05	RS-IS6-75.5	411.36	551	34.1%	52.14
RS-IS8-60	204.48	311	51.9	4.01	RS-IS8-75.5	383.53	515	34.2%	41.84
S-IS0-88.5	329.50	359	−8.2		S-IS0-114	408.19	426	−4.2	
RS-IS0-88.5	774.38	985	27.2%	135.02	RS-IS0-114	1299.43	1445	11.2%	218.34
RS-IS4-88.5	680.91	788	15.7%	106.65	RS-IS4-114	1208.26	1156	−4.3%	196.00
RS-IS6-88.5	656.67	739	12.5%	99.29	RS-IS6-114	1052.02	1084	3.0%	157.73
RS-IS8-88.5	606.11	690	13.8%	83.95	RS-IS8-114	905.02	1011	11.8%	121.72
S-IS0-159	1093.70	1149	−4.8						
RS-IS0-159	2503.70	3501	39.6%	128.92					
RS-IS4-159	2377.63	2801	17.8%	117.39					
RS-IS6-159	2344.13	2626	12.0%	114.33					
RS-IS8-159	2079.69	2451	17.8%	90.15					

For steel pipes, the value of N_c was predominantly consistent with N_e, with errors less than 10%. However, there was a relatively substantial difference between the values of N_e and N_c. It is worth noting that the value of N_e for RS-IS8-60 was lower than that of N_c. The

current specifications in China cannot precisely estimate the bearing capacity of RPC-filled steel tubes with regular dimensions in grid structures, which is not conducive to applying compression members reinforced with RPC.

3.3. Load-Displacement Curves

Figure 12 shows the load-displacement curves of the 25 components where the displacement Δ is the average of the vertical LVDTS. Most of the curves show a descending stage characterized by a negative gradient. The larger the diameter is, the steeper the gradient. The failure process can be divided into three stages:

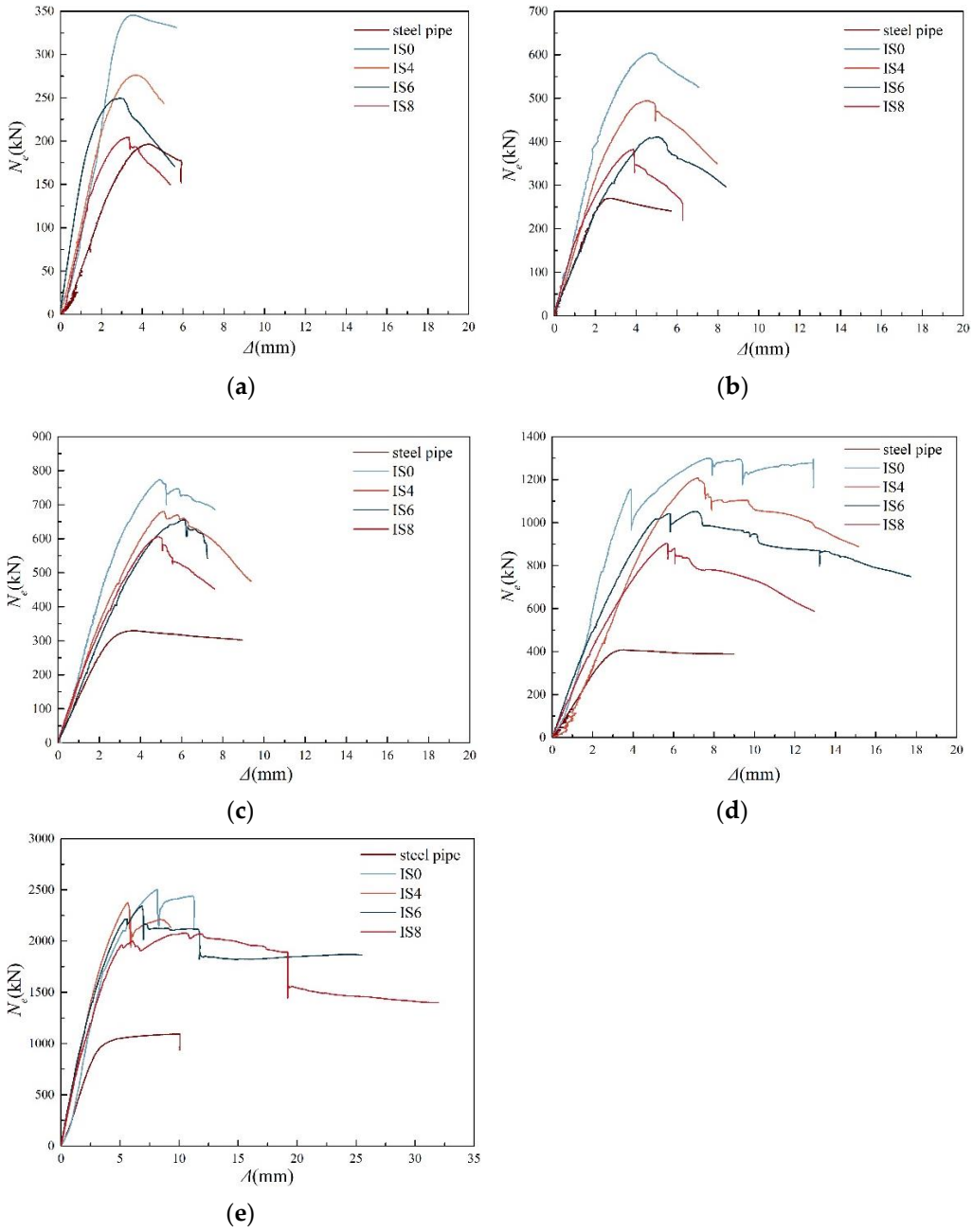

Figure 12. Load-displacement curves. (**a**) ⌀60 × 3.5; (**b**) ⌀75.5 × 3.75; (**c**) ⌀88.5 × 4; (**d**) ⌀114 × 4; (**e**) ⌀159 × 6.

(1) Elastic stage. At the beginning of loading, both the steel and RPC were in the elastic stage, and the curve of N_e vs. Δ increased linearly. No significant deformation appeared on the tube's surface, and as a consequence of different lateral deformation coefficients,

no obvious interaction acted on the two materials. Compared with steel pipes, the elastic stages of the CFST specimens were shortened. This occurred at 70–90% of the peak load but contracted to 60–80% when increasing the prestress.

(2) Elastic-plastic stage. With the increase in load, the materials entered the plastic stage and expanded gradually, followed by a binding of steel and RPC. Thus, the slope of the curve decreased by degrees. Compared with steel pipes, infilled RPC prolonged the elastic-plastic stage of the component, and the effect of initial stress made the steel pipe enter plasticity in advance. With an increase in initial stress, the slope of the curve decreased earlier.

(3) Descending stage. The curve dropped because of the sharp decrease in bearing capacity caused by the lateral bending of bars after peak load. A small confinement coefficient ($\xi \leq 0.69$) of specimens led to less confinement effect from the steel tube, which meant it continued to be loaded onto the core RPC when the steel pipe entered the plastic rheological state. The good ductility of the RPC produced a smooth area in the descending section of the curve, and the inner RPC gradually formed a shear-slip zone along the 45° direction. The curve of the specimen with a large confinement coefficient ($\xi > 0.69$) indicated a typical buckling failure mode, and the plastic zone of the two materials expanded together. With the increase in the lateral bending of the specimen, the load drop was accelerated.

3.4. Stress and Strain Curves

Taking specimen RS-IS6-60 (Figure 13) as an example, the entire section of the steel pipe was compressed at the initial stage of loading, producing the negative longitudinal strain ε_v and the positive hoop strain ε_h with $\varepsilon_v/\varepsilon_h$ equivalent to Poisson's ratio of steel. Figure 14 indicates that the transverse deformation coefficient $\varepsilon_v/\varepsilon_h$ was slightly larger than Poisson's ratio of the steel, which illustrates that the steel pipe was not in an absolute uniaxial compression state, and the bond between the steel and RPC was relatively firm.

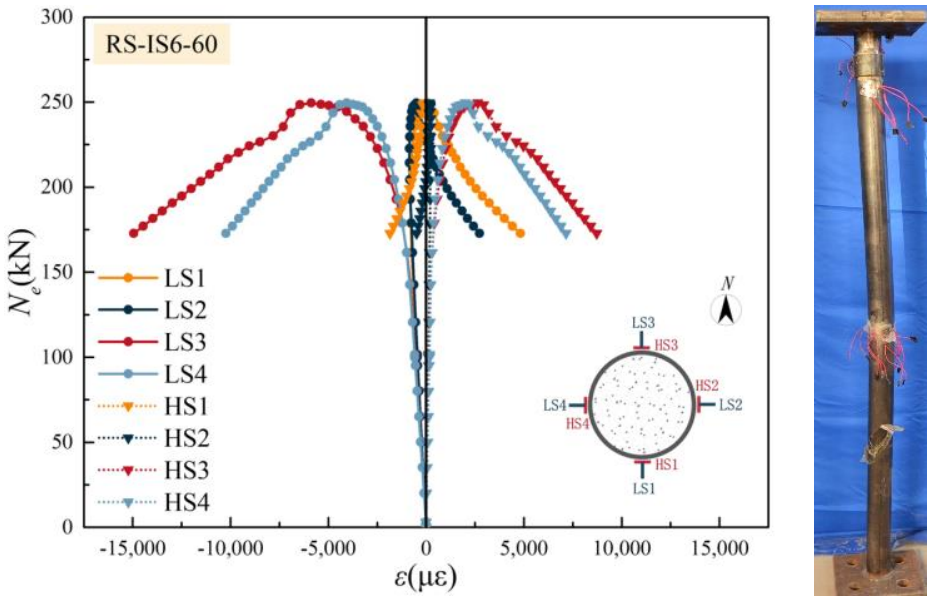

Figure 13. Relationship of N_e to longitudinal and hoop strain (RS−IS6−60).

The initial pressure made the steel enter the elastoplastic state earlier, and the specimen bent toward survey points 1 and 2 so that the longitudinal strain of these two points began to slowly change from the compression state to the tension state, while the hoop tensile strain changed in the opposite direction. Survey points 3 and 4 were still in the longitudinal compressive and hoop tensile states, and the $\varepsilon_v/\varepsilon_h$ began to increase at this point. The hoop strain accounted for the main part, and the constraint effect of the steel pipe on the RPC was strengthened. The strain at survey points 1 and 2 was still in longitudinal

compressive and hoop tension state at the peak load, but the bending degree of the specimen towards survey points 1 and 2 increased rapidly after that. Finally, the longitudinal strain at measuring points 1 and 2 was converted to tensile strain, and the hoop strain was converted to compressive strain. The specimen was then unstable in the directions of measuring points 1 and 2.

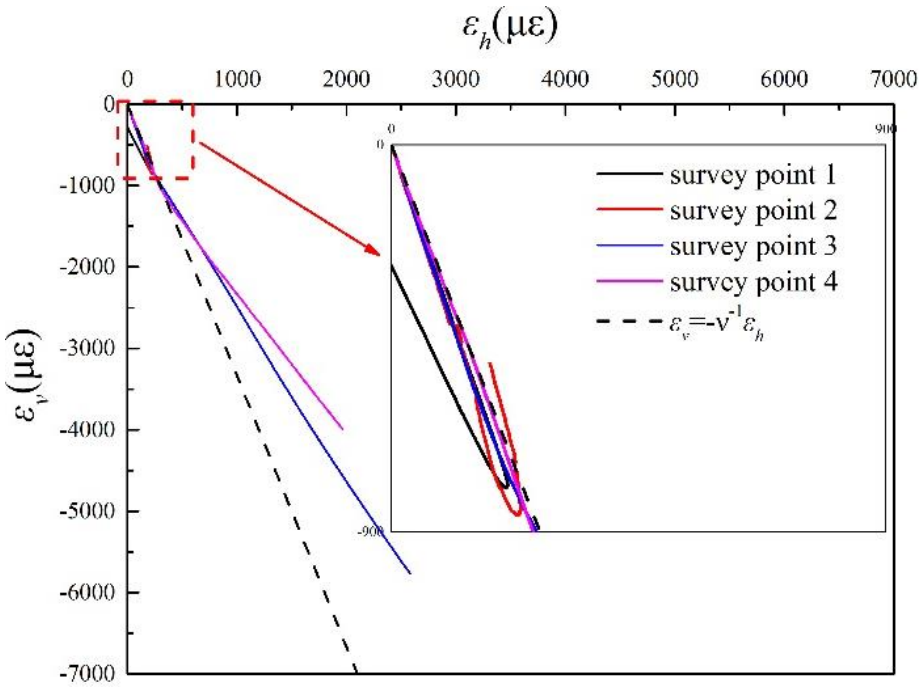

Figure 14. $\varepsilon_v - \varepsilon_h$ curve.

4. Discussion

4.1. Effect of Reinforcement from RPC

Table 4 shows that the bearing capacity of an RPC-filled steel tube is significantly improved compared with an unfilled steel tube in the same section. The RP of the RPC-filled specimens across the five sizes is 75.77, 123.46, 135.02, 162.27, and 218.34%. The results show that the bearing capacity of RPC-filled steel tube members is also greater than that of non-reinforced circular steel tubes with a diameter less than 168 mm or a length-to-diameter ratio greater than 20, proving the feasibility of strengthening the compression members of grid structures with internal pouring concrete.

4.2. Effect of Confinement Coefficient

Generally, under the premise of determining grid size, the lengths of the members in the grid structure were approximately the same, while the diameter was different. In this experiment, when the lengths of the specimens were all 1.5 m, their confinement coefficients were: $\xi_{60} = 1.13$, $\xi_{75.5} = 0.90$, $\xi_{88.5} = 0.76$, $\xi_{114} = 0.51$, and $\xi_{159} = 0.69$. As shown in Figure 15, although the filled RPC can improve the bearing capacity of members, the contribution of reinforcement materials decreases as the hoop coefficient increases.

4.3. Effect of Initial Stress

The initial stress of the steel tube influences the bearing capacity of the rod after reinforcement. As the initial stress increases, the reinforcement effect becomes less and less apparent. Figure 13 shows that the bearing capacity of the ⌀60× 3.5 mm pipe is improved by only 4.01% after infill with the RPC under initial stress of 0.8. Thus, it is recommended to use other methods for reinforcement if the length-to-diameter ratio of the member is greater than 17.5 and the initial stress of the member in the grid structure is large.

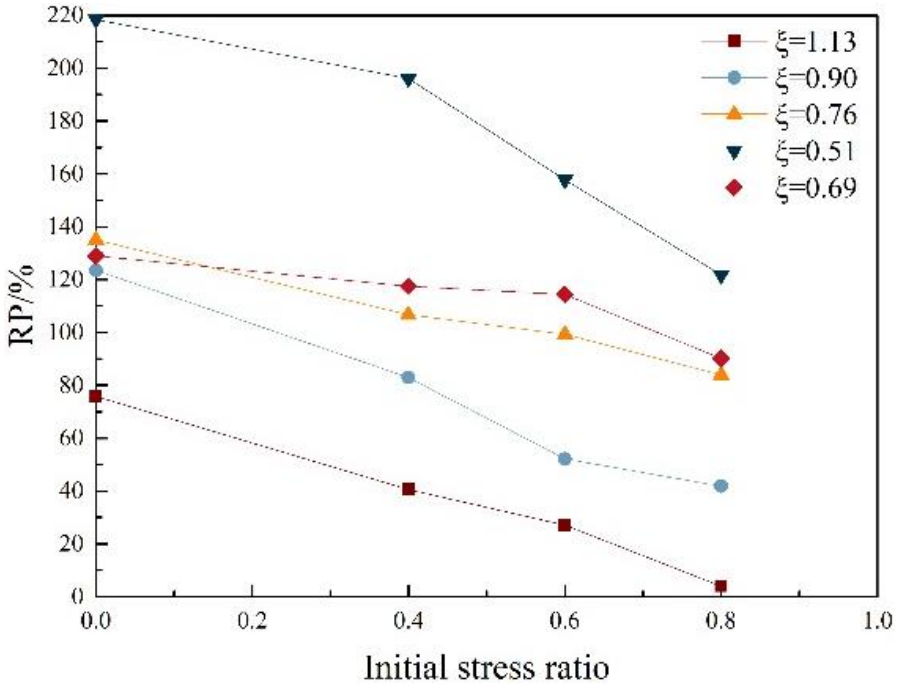

Figure 15. Contribution of RPC.

5. Calculation of Reinforced Bearing Capacity

The structural requirements and the design methods for the bearing capacity of the composite members in the six domestic and foreign codes [12,28,37–40] (hereinafter referred to as "the codes") are listed below, and the bearing capacity of RPC-filled steel tubular members without initial stress in this test is calculated from them. Compared with the test results, the calculation method of axial compression bearing capacity of RPC-reinforced grid structure members is proposed.

5.1. Detailing Requirements

The limit values of material strength, diameter-to-thickness ratio D/t, confinement coefficient ξ, steel contribution factor α_s and material partial coefficient γ in each code are shown in Table 5. f_{ck}, f'_{ck}, and f_y are the characteristic values of the axial compressive strength of concrete, the compressive (cylinder) strength of concrete, and the yield strength of steel, respectively. The f_{ck} is adopted as concrete strength for calculation in Chinese codes, while the f'_{ck} is used in others. To facilitate comparison, the equivalent to the other measure of concrete strength has been given. The γ_c and γ_s represent the partial coefficients of concrete and steel materials, respectively. The calculation methods for the material design strength in each specification are different, and it is uniformly defined as the characteristic value of material strength divided by the γ_c or γ_s. The effective elastic flexural stiffness $(EI)_{eff}$ can be expressed in the form of $E_s I_s + kE_c I_c$ in all codes, which only differs in the value of k.

ξ represents the confinement effect of the steel tube on the infilled concrete and is defined as the ratio of the nominal bearing capacity of the steel tube to that of the concrete ($A_s f / A_c f_c$) in Chinese codes, while other codes represent it as α_s, which is defined as the ratio of the nominal bearing capacity of the steel tube to that of the composite member ($A_s f / (A_s f + A_c f_c)$). In the calculations of both ξ and α_s, A_s and A_c are the cross-sectional areas of the steel pipe and concrete, respectively, and f and f_c are the compressive design strengths of the steel pipe and concrete, respectively.

Table 5. Detailing requirements of relevant standards.

Code	GB 50936 [28]	GB 51367 [12]	EC 4 [38]	AISC [39]	AIJ [40]	AS 2327 [41]
f_{ck}	20.1~50.2	20.1~50.2	16.9~38.5	17.8~51.3	≤41.8	17.8~73.3
f'_{ck}	23.7~70.0	23.7~69.97	20~50	21~70	≤56.4	20~100
f_y	235~460	23.7~69.97	235~460	≤525	235.2~352.8	<690
D/t	$\leq 135\frac{235}{f_y}$	$D \geq 200$; $t \geq 4$	$\leq 90\frac{235}{f_y}$	$\frac{0.15E}{f_y}$	$\leq \frac{1.5 \cdot 240}{f_y/98}$	$\frac{0.15E}{f_y}$
γ_c	1.4	1.4	1.5	1	3/1.5	1
γ_s	1.09~1.125	1.09~1.125	1.15	1	1.5/1.0	1
k	1	1	0.6	C_1	0.2	0.72
ξ	0.5~2.0	-	-	-	-	-
α_s	-	-	0.2~0.9	≥0.01	-	0.2~0.9

Note: $C_1 = 0.1 + 2\left(\frac{A_s}{A_s + A_c}\right) \leq 0.3$.

5.2. Calculation Methods

1. GB 50936-2014 [28]

The calculation method of the bearing capacity of concrete-filled steel tubes in Chapter VI of GB 50936-2014 is shown as follows:

$$N \leq N_u \tag{2}$$

$$N_u = \varphi_l \varphi_e N_0 \tag{3}$$

$$N_0 = \begin{cases} 0.9A_c f_c(1 + \alpha\xi) & \left(\xi \leq 1/(\alpha - 1)^2\right) \\ 0.9A_c f_c\left(1 + \sqrt{\xi} + \xi\right) & \left(\xi > 1/(\alpha - 1)^2\right) \end{cases} \tag{4}$$

$$\xi = \frac{A_s f}{A_c f_c} \tag{5}$$

$$\varphi_l = \begin{cases} 1 & (L_e/D \leq 4) \\ 1 - 0.0226(L_e/D - 4) & (4 < L_e/D \leq 30) \\ 1 - 0.115\sqrt{L_e/D - 4} & (L_e/D > 30) \end{cases} \tag{6}$$

$$\varphi_e = \begin{cases} \frac{1}{1 + 1.85\frac{e_0}{r_c}} & (e_0/r_c \leq 1.55) \\ \frac{1}{3.92 - 5.16\varphi_l + \varphi_l \frac{e_0}{0.3r_c}} & (e_0/r_c > 1.55) \end{cases} \tag{7}$$

In the equations above, N is the design value of axial pressure on members, N_u is the design value of the axial compression bearing capacity, N_0 is that of the axial compression bearing capacity of stub columns, φ_l is the reduction coefficient of slenderness ratio, L_e is the effective length, φ_e is the reduction coefficient of eccentricity, α is a factor related to concrete grades, e_0 is the larger eccentricity of the member, and r_c is the section radius of filled concrete.

2. GB 51367-2019 [12]

The formulae in GB 51367-2019 relate to those in GB 50936-2014 but consider the effect of initial stress in the steel tube and include multiplying by the reinforcement strength correction coefficient η_c, when N_0 is calculated:

$$N_0 = \begin{cases} 0.9\eta_c A_c f_c(1 + \alpha\xi) & \left(\xi \leq 1/(\alpha - 1)^2\right) \\ 0.9\eta_c A_c f_c\left(1 + \sqrt{\xi} + \xi\right) & \left(\xi > 1/(\alpha - 1)^2\right) \end{cases} \tag{8}$$

$$\eta_c = \begin{cases} 0.85 & (\sigma_{0max}/f \leq 0.2) \\ 0.8 & (0.2 < \sigma_{0max}/f \leq 0.4) \\ 0.75 & (0.4 < \sigma_{0max}/f \leq 0.65) \\ 0.7 & (\sigma_{0max}/f > 0.65) \end{cases} \tag{9}$$

where σ_{0max} is the maximum nominal stress.

3. EC 4 [37]

Here the equations of a composite member under compression in EC 4 are given:

$$N \le \chi N_0 \tag{10}$$

$$N_0 = \begin{cases} A_s f + A_c f_c' & (\overline{\lambda} > 0.5) \\ \eta_a A_s f + A_c f_c' \left(1 + \eta_c \frac{t}{D} \frac{f_y}{f_{ck}'}\right) & (\overline{\lambda} \le 0.5) \end{cases} \tag{11}$$

$$\eta_a = 0.25(3 + 2\overline{\lambda}); \eta_c = \eta_{c0} = 4.9 - 18.5\overline{\lambda} + 17\overline{\lambda}^2 \tag{12}$$

$$\overline{\lambda} = \sqrt{\frac{N_0}{N_{cr}}};\ N_{cr} = \frac{\pi^2 (EI)_{eff}}{L^2} \tag{13}$$

χ is a reduction factor for the relevant buckling mode, $\overline{\lambda}$ is the relative slenderness, f_c' is the concrete cylinder strength design value, and N_{cr} is the elastic critical normal force.

4. AISC [39]

$$N = \Phi_c N_u = 0.75 N_u \tag{14}$$

$$N_u = \begin{cases} N_0 \cdot 0.658^{\frac{N_0}{N_{cr}}} & (N_0/N_{cr} \le 2.25) \\ 0.877 N_0 & (N_0/N_{cr} > 2.25) \end{cases} \tag{15}$$

$$N_0 = A_s f + 0.85 A_c f_c' \tag{16}$$

In the above, Φ_c is the resistance factor for axially loaded composite columns.

5. AIJ [40]

AIJ includes allowable stress design and limits state design methods. The latter one was used for calculations in this paper:

$$N_u = \begin{cases} N_{u1}, & L_e/D \le 4 \\ N_{u1} - 0.125(N_{u1} - N_{u2})(L_e/D - 4), & 4 < L_e/D \le 12 \\ N_{u2}, & L_e/D > 12 \end{cases} \tag{17}$$

$$N_{u1} = 0.85 A_c f_c' + 1.27 A_s \cdot f_y \tag{18}$$

$$N_{u2} = N_{ccr} + N_{scr} \tag{19}$$

N_{u1} and N_{u2} are the ultimate compressive bearing capacity calculated according to the short column ($L_e/D = 4$) and the long column ($L_e/D = 12$), respectively; and N_{ccr} and N_{scr} are the critical loads of the concrete and steel tube, respectively.

6. AS/NZS 2327 [41]

The calculation equations for compressive CFST in AS/NZS 2327 are shown below:

$$N_u = \alpha_c N_0 \le N_0 \tag{20}$$

$$N_0 = \begin{cases} 0.9 A_s f + 0.65 A_c f_c' & (\lambda_r > 0.5) \\ 0.9 \eta_a A_s f + 0.65 A_c f_c' \left(1 + \eta_c \frac{t}{D} \frac{f_y}{f_{ck}'}\right) & (\lambda_r \le 0.5) \end{cases} \tag{21}$$

$$\alpha_c = \xi \left[1 - \sqrt{1 - \left(\frac{90}{\xi \lambda}\right)^2}\right],\ \xi = \frac{\left(\frac{\lambda}{90}\right)^2 + 1 + \eta}{2\left(\frac{\lambda}{90}\right)^2},\ \eta = 0.00326(\lambda - 13.5) \ge 0 \tag{22}$$

$$\lambda = \lambda_\eta - 0.5 \frac{2100(\lambda_\eta - 13.5)}{{\lambda_\eta}^2 - 15.3\lambda_\eta + 2050},\ \lambda_\eta = 90\lambda_r,\ \lambda_r = \sqrt{\frac{N_s}{N_{cr}}} \tag{23}$$

$$N_s = A_s f + A_c f_c' \tag{24}$$

Here α_c is the compression member slenderness reduction factor.

5.3. Data Fitting

The test results in this paper show that the failure mode of RPC-filled steel tubular members, approximately 1.5 m in length and 60–159 mm in diameter, presents as an elastic-plastic instability state of the extreme point type. The constraint effect of the steel tubes on concrete is ignored when calculating the axial compression bearing capacity of members with a large length-to-diameter ratio in several codes; therefore, we recommend using the stable nominal bearing capacity (Equation (25)) as the axial compression bearing capacity of the composite member in the grid structure. The experimental result specimens without initial stress are compared with the calculation results of the national codes and shown in Figure 16a.

$$N_{nom} = \varphi_l (A_s f + A_c f_c) \tag{25}$$

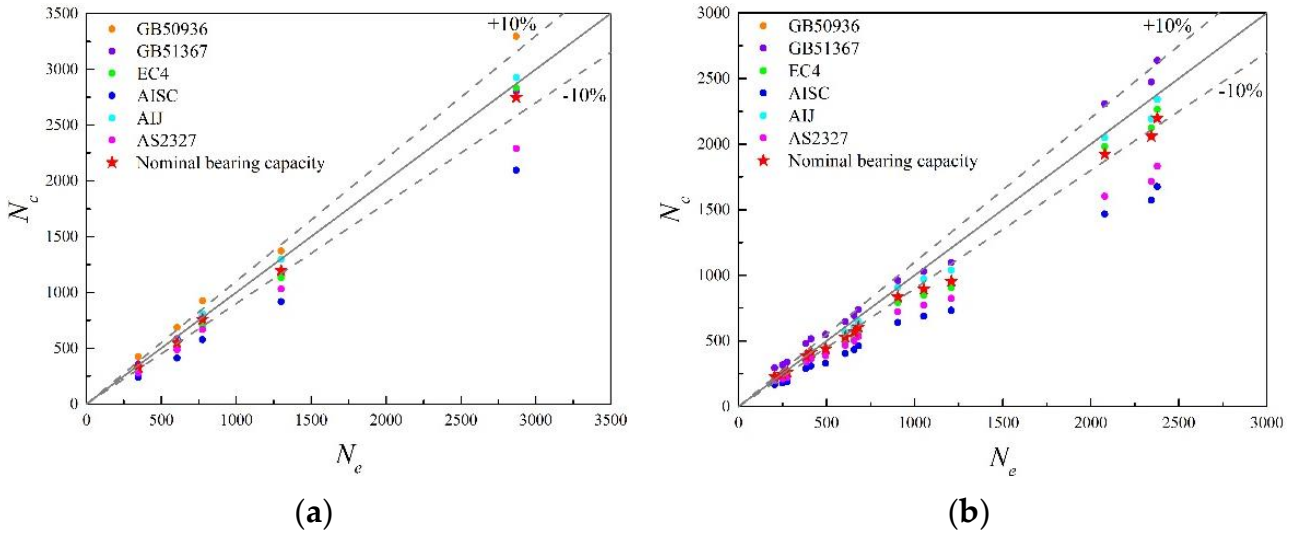

Figure 16. Comparison of design values and test results. (**a**) composite members without prepress; (**b**) composite members with prepress.

For the specimens with initial stress, the strength correction factor η_c proposed in GB 51367 [12] was used to revise the calculated values of the national codes above. The calculated results are shown in Figure 16b, and the nominal bearing capacity of stability is corrected to

$$N_{nom} = \varphi_l \eta_c (A_s f + A_c f_c) \tag{26}$$

The experimental results and parameters from a total of 202 RPC-filled steel tubular stub columns [17,18,21,42–50] and 40 long columns [21,22,46,50] are displayed in Table 6. In these pre-existing results, the maximum length-to-diameter ratio of each specimen is 12, significantly less than that of the grid structure members researched above, and no initial stress acts on these specimens. The mean and standard deviation of the ratios of the calculated capacities (according to the codes) to the experimental capacities (from this paper) and the 242 results conducted in past studies are listed in Figure 17.

Table 6. Parameter range of tested specimen.

D	*t*	*f*	f_c	*L*/*D*	ξ
83~219	1~16	244.9~453	53.19~154	2.65~12	0.057~3.133

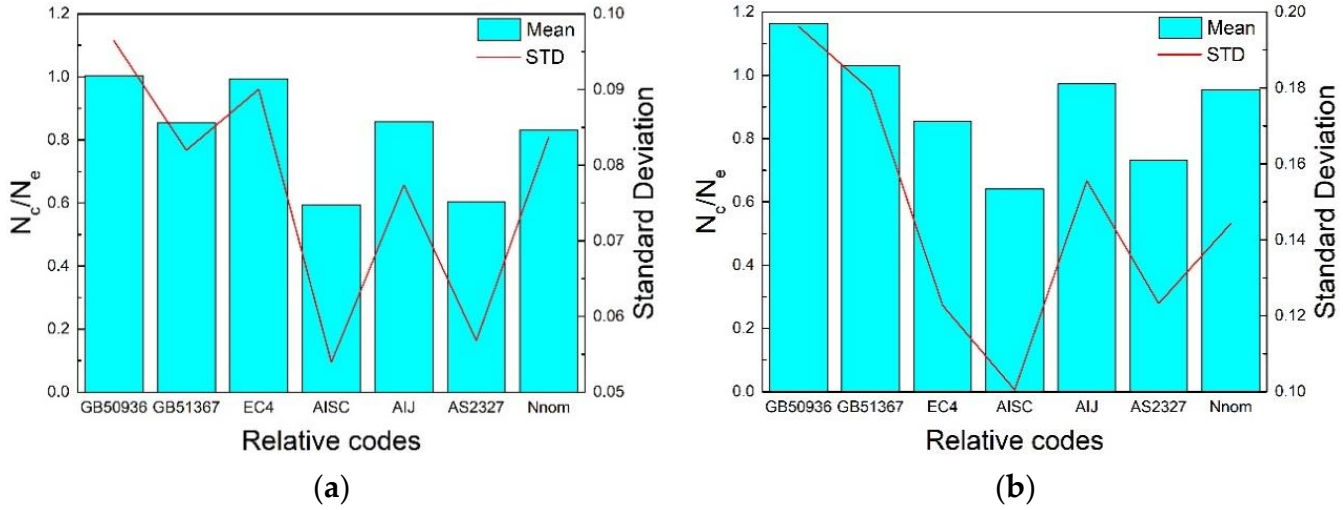

Figure 17. Comparison of specific values and standard deviation. (**a**) stub columns; (**b**) medium long and long columns.

For RPC-filled steel tubular short columns, the mean values of N_c/N_e calculated by each of the six codes are 1.00, 0.85, 0.99, 0.59, 0.86, 0.60, and 0.83, and the standard deviations are 0.096, 0.082, 0.090, 0.054, 0.077, 0.057, and 0.084. Compared with GB 50936 [28], the estimated values of GB 51367 [12] are more conservative because the test results without initial stress are required to be reduced by $\eta_c = 0.85$ in GB 51367.

For relatively long RPC-filled steel tubular columns, the mean values of N_c/N_e calculated by the six codes are 1.16, 1.03, 0.85, 0.64, 0.97, 0.73, and 0.96, and the standard deviations are 0.196, 0.179, 0.123, 0.100, 0.156, 0.123, and 0.144. GB 51367, AIJ and N_{nom} are the most accurate in predicting the bearing capacity of members, and of the two, the deviation of N_{nom} is the lowest. Thus, it is suggested that the N_{nom} defined in Equation (26) is taken as the ultimate bearing capacity when $L_e/D > 4$ and otherwise use GB 51367 [12].

6. Conclusions

The experimental research on the axial compression bearing capacity of 25 grid structure members with different sizes, initial stress ratios, and cross-sectional forms was presented. The reinforcement process of grid members was simulated, which verified the operability of the reinforcement method proposed in this paper. The following conclusions can be drawn:

(1) The method of strengthening compressive members in a grid structure by infilling RPC effectively enhances the bearing capacity. RPC and initial stress in the steel tubes did not change the final failure mode of specimens. With the decrease of the confinement coefficient ξ or the initial pressure, the contribution of the reinforcement material can reach up to 218.34%, fully proving the superiority of the reinforcement method in this paper.

(2) For length-to-diameter ratios of 6.60~17.5, all members show elastic-plastic instability failure. In the descending section of the bearing capacity, oblique shear failure appeared at the bottom of the reinforced specimens with $\xi \leq 0.69$, while the specimens with a larger hoop coefficient exhibited only instability failure. There is no local buckling around the grouting hole of reinforced specimens, and it is suggested that the necessary measures in this paper, including using steel glue, should be used to repair the grouting hole.

(3) The variation tendency of longitudinal and hoop strains in the middle of the steel tube throughout the loading process is consistent with the bending direction of the steel tube. At the beginning of the loading, the whole section of the steel tube is compressed while the longitudinal strain of steel tubes gradually decreases and changes from compressive to tensile strain as the load increases. At the end of the loading, half of the steel tube section is compressed, and half is tensioned, which presents a typical instability failure.

(4) Regarding the test results in this paper and 242 from past research, a comparison of calculated bearing capacity from six domestic and foreign codes was carried out. The results indicate that the axial compression calculation method of composite members given by those national codes cannot accurately estimate the bearing capacity of RPC-filled steel tubular members. The nominal bearing capacity $N_{nom} = \varphi_l \eta_c (A_s f + A_c f_c)$ should be adopted as the ultimate capacity of compressed members reinforced by RPC in grid structures.

Author Contributions: Conceptualization, Y.D. and H.L.; methodology, Y.D.; software, Y.D.; validation, Y.D., Y.Z. and S.J.; resources, S.J.; data curation, Y.D. and Y.Z.; writing—original draft preparation, Y.D.; writing—review and editing, Y.Z.; visualization, Y.D.; supervision, H.L. and S.J.; project administration, Y.D. and S.J.; funding acquisition, H.L. All authors have read and agreed to the published version of the manuscript.

Funding: This research was funded by National Nature Science Foundation of China grant number No. 51578357.

Conflicts of Interest: The authors declare no conflict of interest.

References

1. Dong, S.; Zhao, Y.; Xing, D. Application and development of modern long-span space structures in China. *Spat. Struct.* **2012**, *18*, 3–16. (In Chinese) [CrossRef]
2. Dong, S.; Zhao, Y.; Zhou, D. New Structural Forms and New Technologies in the Development of Steel Space Structures in China. *Adv. Struct. Eng.* **2000**, *3*, 49–65. [CrossRef]
3. Zhang, Y.; Xue, S.; Yang, Q. *Long-Span Spatial Structure*, 2nd ed.; Mechanical Industry Press: Beijing, China, 2014; Volume 386. (In Chinese)
4. Ge, L. *The Analysis of Collapse of a Welded Hollow Ball Rack Workshop*; Taiyuan University of Technology: Taiyuan, China, 2014. (In Chinese)
5. Tang, D.; Zhang, L.; Wei, X.; Juan, L.U. Grid Structure Appraising and Reinforce Reconstruction by SAP2000 Static Non-Linear Analysis. *Constr. Qual.* **2013**, *31*, 25–28. (In Chinese)
6. Jian, L.; Lei, H.G. Analysis on the Causes of Fatigue Accidents of a Bolt-Ball Structure Plant in Shanxi. *Appl. Mech. Mater.* **2016**, *851*, 864–869.
7. Xing, J.H.; Lu, M.; Li, H.W.; Zhao, Y.M.; Yu, Y. The Seismic Damage Investigation and Phenomenon Analysis of Space Grid Structures in Lushan Ms 7.0 Earthquake. In *Advances in Civil and Structural Engineering III*; PTS 1-4; Trans Tech Publications Ltd.: Bäch SZ, Switzerland, 2014; Volume 501–504, p. 1535.
8. Dai, J.; Zhe, Q.; Zhang, C.; Weng, X. Preliminary investigation of seismic damage to two steel space structures during the 2013 Lushan earthquake. *Earthq. Eng. Eng. Vib.* **2013**, *12*, 497–500. [CrossRef]
9. Lei, H. *Analysis and Treatment of Steel Structure Accidents*; China Building Materials Industry Press: Beijing, China, 2003. (In Chinese)
10. Wang, J. Collapse of Shenzhen International Exhibition Center. *Build. Struct.* **1993**, *12*, 37. (In Chinese)
11. Li, Z.; Li, L.; Shi, Y.; Huang, X. Failure analysis of light rail station structure at Donghai Road in the "Aug 12th" accident of great fire explosion at Tianjin Port. *J. Build. Struct.* **2019**, *40*, 1–7. (In Chinese)
12. *GB 51367-2019*; Standard for Design of Strengthening Steel Structure. China Ministry of Construction: Beijing, China, 2019. (In Chinese)
13. Han, L.H.; Wei, L.; Reidar, B. Developments and advanced applications of concrete-filled steel tubular (CFST) structures: Members. *J. Constr. Steel Res.* **2014**, *100*, 221–228. [CrossRef]
14. Chen, B.; Li, L.; Luo, X.; Wei, J.; Lai, X.; Liu, J.; Ding, Q.; Li, C. Review on ultra-high strength concrete filled steel tubes. *J. Traffic Transp. Eng.* **2020**, *20*, 1–21. (In Chinese)
15. An, L.; Ekkehard, F. A review and analysis of circular UHPC filled steel tube columns under axial loading. *Struct. Eng. Mech.* **2017**, *62*, 417–430.
16. Pierre, R.; Cheyrezy, M. Composition of reactive powder concretes. *Cem. Concr. Res.* **1995**, *25*, 1501–1511.
17. Wang, Q.; Shi, Q.; Lui, E.M.; Xu, Z. Axial compressive behavior of reactive powder concrete-filled circular steel tube stub columns. *J. Constr. Steel Res.* **2019**, *153*, 42–54. [CrossRef]
18. Rong, Q.; Zeng, Y.; Guo, L.; Hou, X.; Zheng, W. Response of RPC-Filled Circular Steel Tube Columns under Monotonic and Cyclic Axial Loading. *Shock. Vib.* **2019**, *2019*, 9141592. [CrossRef]
19. Lai, Z.; Yao, P.; Huang, W.; Chen, B.; Ying, Z. Reactive powder concrete-filled steel tube (RPCFT) members subjected to axial tension: Experimental study and design. *Structures* **2020**, *28*, 933–942. [CrossRef]
20. Xiong, M.X.; Xiong, D.X.; Liew, J.Y.R. Behaviour of steel tubular members infilled with ultra high strength concrete. *J. Constr. Steel Res.* **2017**, *138*, 168–183. [CrossRef]

21. Yao, L. *Researches on Behavior of Eccentrically Loaded Stub Column and Axially Compressed Slender Column with RPC-Filled Circular Steel Tube*; Fuzhou University: Fuzhou, China, 2005. (In Chinese)
22. Ji, W.; Luo, H.; Yang, G. Experimental study on axial compression behavior of reactive powder concrete filled steel tubular long columns. *China Railw. Sci.* **2014**, *35*, P28–P33. (In Chinese)
23. Wei, Z.; Liu, X. Application of ceramic concrete filled steel tube in grid structure. *Metall. Constr. Technol. Manag.* **1993**, *9*, 14–18. (In Chinese)
24. Chen, X.; Liu, X. Experimental study on composite grid of ceramic concrete filled steel tube. *J. Harbin Univ. Civ. Eng. Archit.* **1995**, *28*, P154–P159. (In Chinese)
25. Gao, R.; Zheng Liu, Z.; Wu, M. Static Linear Analysis of Concrete-Filled Steel Tubular Composite Grid Structure. *J. Ningxia Inst. Technol.* **1996**, *S1*, 197–203. (In Chinese)
26. Pan, W. Concrete-Filled Steel Tube Reticulated Shell Seismic Analysis. Master's Thesis, Xi'an University of Architecture and Technology, Xi'an, China, 2008. (In Chinese).
27. Duan, Y.; Lei, H. Comparison for Solid Concrete-filled Circular Steel Tubes Load-carrying Capacities in Frame Structures Basing on Chinese codes. *J. Phys. Conf. Ser.* **2021**, *2011*, 12044.
28. *GB 50936-2014*; Technical Code for Concrete Filled Steel Tubular Structures. China Ministry of Construction: Beijing, China, 2014. (In Chinese)
29. Luo, H.; Wang, W.; Wang, G.; Pang, B. Study of Circular Reactive Powder Concrete-Filled Steel Tube Stub Columns under Axial Compression. *J. Eng. Sci. Technol. Rev.* **2018**, *11*, 144–152. [CrossRef]
30. Chen, M.; Hou, X. Comparative Study on the Axial Compression and Bearing Capacity of Reactive Powder Concrete-Filled Circular Steel Tube. *Adv. Mater. Sci. Eng.* **2018**, *2018*, 1–11. [CrossRef]
31. Li, B.; Zhang, L.; Gao, C. Steel tube concrete short columns and long column bounds slenderness ratio test. *Concrete* **2018**. (In Chinese)
32. *GB 50017-2017*; Standard for Design of Steel Structures. Ministry of Housing and Urban-Rural Development of the People's Republic of China: Beijing, China, 2017. (In Chinese)
33. Wu, P. *Study of Mechanical Properties of Steel Tube Filled with Self-Compacting RPC*; Beijing Jiaotong University: Beijing, China, 2010. (In Chinese)
34. *GB/T 228.1-2010*; Metallic Materials-Tensile Testing—Part 1: Method of test at Room Temperature. China Standard Press: Beijing, China, 2010. (In Chinese)
35. *GB/T 2975-2018*; Steel and Steel Products-Location and Preparation of Samples and Test Pieces for Mechanical Testing. China Standard Press: Beijing, China, 2018. (In Chinese)
36. *GBT 31387-2015*; Reactive Powder Concrete. China Standard Press: Beijing, China, 2015. (In Chinese)
37. *GB/T 50081-2019*; Standard for Test Methods of Concrete Physical and Mechanical Properties. Ministry of Construction: Beijing, China, 2019. (In Chinese)
38. *EN1994-1-1*; Design of Composite Steel and Concrete Structures—Part 1-1: General Rules and Rules for Buildings. CEN: Brussels, Belgium, 2004.
39. *ANSI/AISC 360-10*; Specification for Structural Steel Buildings. AISC: Chicago, IL, USA, 2010.
40. *Concret-Filled Steel Pipe Structure Design and Construction Guidelines*; Japan Architectural Institute: Tokyo, Japan, 1997. (In Japanese)
41. *AS/NSZ 2327:2017*; Composite Structures-Composite Steel-Concrete Construction in Buildings. SAI Global Limited: Sydney, Australia; Wellington, New Zealand, 2017.
42. Xu, Z. *Experimental Study and Analysis of RPC—Filled Steel Tube under Axial Compression and Push Out Test*; Hunan University: Hunan, China, 2016. (In Chinese)
43. Yang, G. *Research on Behavior and Ultimate Bearing Capacity of Reactive Powder Concrete-Filled Steel Tube Columns under Axial Compression*; Beijing Jiaotong University: Beijing, China, 2013. (In Chinese)
44. Feng, J. *Study on Mechanical Behavior of Reactive Powder Concrete Filled Steel Tubular Columns*; Tsinghua University: Beijing, China, 2008. (In Chinese)
45. Lin, Z.; Wu, Y.; Shen, Z. Research on behavior of RPC filled circular steel column subjected to axial compression. *J. Build. Struct.* **2005**, *26*, 52–57. (In Chinese)
46. Yang, W. *Study on Mechanical Properties and Ultimate Bearing Capacity of Reactive Powder Concrete Filled Steel Tube*; Hunan University: Changsha, China, 2003. (In Chinese)
47. Zhang, J. *Experimental Investigation on Behavior of Reactive Powder Concrete Filled Steel Tube Columns*; Fuzhou University: Fuzhou, China, 2003. (In Chinese)
48. Luo, H. *Study on Axial Compression Behavior of Reactive Powder Concrete Filled Circular Steel Tube Short Columns*; Beijing Jiaotong University: Beijing, China, 2011. (In Chinese)
49. Yan, Z.G.; Yan, H.; An, M.Z. Axial Compression Experimental Research of RPC Filled Steel Tube Columns. *Adv. Mater. Res.* **2010**, *150*, 198–202. [CrossRef]
50. Zeng, J. Research on Behavior of Eccentrically Loaded Slender Column of Circular Steel Tube. Master's Thesis, Fuzhou University, Fujian, China, 2005. (In Chinese).